Ion Motion Induced Emittance Growth of Matched Electron Beams in Plasma Wakefields

Weiming An, Wei Lu, Chengkun Huang, Xinlu Xu, Mark J. Hogan, Chan Joshi, and Warren B. Mori

Phys. Rev. Lett. **118**, 244801 — Published 14 June 2017

DOI: 10.1103/PhysRevLett.118.244801

Ion motion induced emittance growth of matched electron beams in plasma wakefields

Weiming An,[1,2,*] Wei Lu,[3,4] Chengkun Huang,[5] Xinlu Xu,[1,2] Mark J. Hogan,[6] Chan Joshi,[1] and Warren B. Mori[1,2]

[1]*Department of Electrical Engineering, University of California Los Angeles, Los Angeles, CA 90095, USA*
[2]*Department of Physics and Astronomy, University of California Los Angeles, Los Angeles, CA 90095, USA*
[3]*Department of Engineering Physics, Tsinghua University, Beijing 100084, China*
[4]*IFSA Collaborative Innovation Center, Shanghai Jiao Tong University, Shanghai 200240, China*
[5]*Los Alamos National Laboratory, Los Alamos, New Mexico 87545, USA*
[6]*SLAC National Accelerator Laboratory, Menlo Park, California 94025, USA*

(Dated: March 27, 2017)

Plasma based acceleration (PBA) is being considered as the basis for building a future linear collider. Nonlinear plasma wakefields have ideal properties for accelerating and focusing electron beams. Preservation of the emittance of nano Coulomb beams with nanometer scale matched spot sizes in these wakefields remains a critical issue due to ion motion caused by their large space charge forces. We use fully resolved quasi-static particle-in-cell simulations of electron beams in hydrogen and lithium plasmas, including when the accelerated beam has different emittances in the two transverse planes. The projected emittance initially grows and rapidly saturates with a maximum emittance growth of less than 80% in hydrogen and 20% in lithium. The use of over focused beams is found to dramatically reduce the emittance growth. The underlying physics that leads to the lower than expected emittance growth are elucidated.

PACS numbers: 52.40.Mj, 52.59.Bi, 52.59.Fn

There has been tremendous recent progress on plasma-based acceleration (PBA) where charged particles are accelerated by plasma wakefields[1–8]. This has led to the consideration of designing a future linear collider (LC) using particle beams or lasers to drive the wakefields [9–11]. With respect to particle beam-driven plasma wakefield acceleration (PWFA), this progress includes demonstrating sustained high gradient acceleration (∼50 GeV/m) over one meter[5], efficient transfer of energy from the wake to the trailing beam[6] and high gradient positron acceleration in self-loaded wakes[8]. For future LC designs it is also necessary that the luminosity, $L = \frac{fN^2}{4\pi\sigma_x\sigma_y}$ be large, where N is the number of particles in each bunch, f is the frequency of the collisions, and $\sigma_{x,y}$ is the spot size of the bunch at the interaction point. In order to focus a bunch to the spot size needed to achieve luminosities $\sim 10^{34}\,\mathrm{cm}^{-2}\cdot\mathrm{s}^{-1}$, the bunch should have a normalized emittance, ϵ_N, of $\sim 100\,\mathrm{nm}$ and $\sim 1\,\mathrm{nC}$ of charge.

Much research in PBA has been on nonlinear wakefields [12–14] because they have ideal properties for accelerating and focusing electron beams with nC of charge. They are described by complete electron blowout. The blown out electrons form a narrow sheath with the shape of a "bubble" that surrounds the plasma ions. If the wake is axisymmetric and plasma ions do not move, the focusing field can be shown to be $F_f = m_e\omega_p^2 r/2$ [12–14], which is proportional to r and independent of $\xi = ct - z$, where ω_p is the plasma frequency. Unless specified, henceforth we normalize length to $c/\omega_p \equiv k_p^{-1}$, time to $1/\omega_p$, mass to the electron mass, m_e, and charge to e. For central forces that are linear in r, the forces in the $\hat{x}$ and $\hat{y}$ directions are also linear in x and y respectively. The matched spot size is $\sigma_r = (2\epsilon_N^2/\gamma)^{1/4}$ [15], where γ is the relativistic Lorentz factor of the beam, which corresponds to 100 nm size beams for the emittances required to reach the luminosities of future LC parameters.

In [16] it was shown that for tightly focused nC class beams the Coulomb field can pull the ions inward during the transit time of the beam. Essentially, when $n_b/n_0 >> m_i/m_e$ (where n_0 is the plasma density) the ion density is compressed, which perturbs the focusing force, $F_f = r/2 + \tilde{F}_f$ potentially causing catastrophic emittance growth. In [17] it was proposed to adiabatically match the beam to the perturbed focusing field by using plasma sections with decreasing plasma ion masses. However, there has been little work on quantifying the emittance growth from the ion motion itself because the simulations need to be self-consistent and resolve the small spot sizes of the beam while including the much larger size of the bubble.

In this letter, we investigate the ion motion-induced emittance growth through the use of highly resolved QuickPIC [18, 19] simulations and single particle calculations in parameterized focusing fields. QuickPIC is a three-dimensional quasi-static particle-in-cell code, which is used to efficiently model short-pulse laser and particle beam plasma interactions [20]. The results show that even though the ion density compression within the e^- bunch is large, the emittance growth is modest because the ion collapse is only strong in the core of the beam, the single particle orbits are highly anharmonic, and the ion collapse varies along the bunch length. We also find that over focusing the accelerated bunch (using a spot size less than the matched spot size) can also dramatically reduce the emittance growth.

We start by studying how a given longitudinal slice of

the trailing beam evolves in prescribed nonlinear focusing fields due to an ion density peak on axis of the form $n_{ion}/n_0 = 1 + A\exp(-r^2/2\sigma^2)$, for which the corresponding focusing force is $F_f = (r/2 + A\sigma^2\frac{1-\exp(-r^2/2\sigma^2)}{r})\hat{r}$. For nonlinear forces the motion in the $\hat{x}$ and $\hat{y}$ directions are coupled. For simplicity, we begin by considering motion only in $\hat{x}$ direction (we also neglect to lowest order the changes to γ), i.e., we consider particles with $y = p_y = 0$. They feel the maximum $|\vec{F}_f \cdot \hat{x}|$ compared to those at the same x but different y and p_y and hence have the largest perturbation on their phase space distribution. We rely on the numerical simulations to include the coupling between the two planes and changes to γ. The insight gained from the 1D model is born out in the simulations.

We use the particle push in QuickPIC to simulate the evolution of a slice of a beam in a plasma with $n_0 = 1.0 \times 10^{17}\text{cm}^{-3}$. The beam slice has an initial normalized emittance $\epsilon_{Nx0} = 0.1\,\mu$m, where $\epsilon_{Nx} \equiv \sqrt{<x^2><p_x^2> - <xp_x>^2}$ (p_x is normalized to $m_e c$) and the $<>$ represents an average over particles. The initial spot size is $\sigma_{x0} = 0.104\,\mu$m and initial energy is 25 GeV so that the beam is initially matched to the $x/2$ focusing field. We choose the width of the ion density peak as $\sigma = 0.104\,\mu$m, which was set equal to σ_{x0}. The energy of the beam particles is kept constant. In fig. 1a, we plot

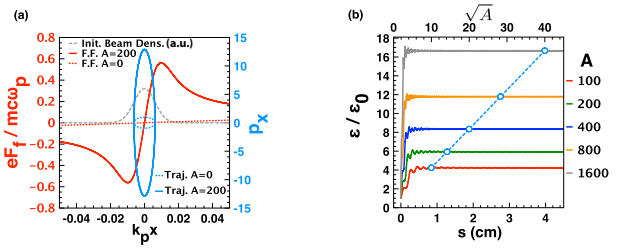

FIG. 1. Emittance evolution of a beam slice in a fixed nonlinear focusing field: (a) Initial beam density profile in arbitrary units (grey dashed line), focusing field (F. F. the red line with A=200 and the red dashed line with A=0) and the particle trajectories (Traj.) in the focusing field of A = 200 (the blue solid line) and A = 0 (the blue dashed line); (b) the slice beam emittance evolution and the emittance growth versus $\sqrt{A}$.

the phase space trajectories, x-p_x, for a particle initially located at $x = \sigma_{x0}$, $p_x = 0$ and under focusing fields with A=0 and A=200 respectively.

When the focusing field is perfectly linear (i.e., A=0), the maximum momentum p_{x0} of the particle equals to 0.964 , which satisfies $\sigma_{x0} \cdot p_{x0} = \epsilon_{Nx0}$ because the slice beam is matched. When there is ion collapse, p_{x0} will be larger because $|F_f|$ is larger. As shown in fig. 1a, p_{x0} increases approximately by a factor of $\sqrt{A} \approx 14.2$ since the slope of the focusing field inside the beam center is around A times larger. Since F_f is nonlinear, the saturated emittance growth will also scale with $\sqrt{A}$ with a proportionality constant less than unity that depends on σ/σ_{x0}. In fig. 1b we plot the emittance growth for different A's but with the same σ/σ_{x0}, and the saturated emittance is seen be roughly $0.425\sqrt{A}$. This scaling of emittance growth with $\sqrt{A}$, i.e., with the square root of the peak ion density would be catastrophic.

However, this is not what is observed in properly resolved self-consistent simulations. We consider the following beam loading scenario where a drive beam with 3.0×10^{10} electrons transfers energy to a trailing beam with 1.0×10^{10} electrons [9, 21]. The drive and trailing beams have $\epsilon_{Nd} = 1\,\text{mm}$ and $\epsilon_{Nt} = 0.1\,\mu$m respectively. The emittance of the trailing beam is chosen to achieve the necessary luminosity of a LC [10]. Both the drive and the trailing beams have an initial energy of 25 GeV and a bi-Gaussian density profile, $\sim e^{-r^2/(2\sigma_r^2)}e^{-z^2/(2\sigma_z^2)}$. The plasma density is $n_0 = 1.0 \times 10^{17}\text{cm}^{-3}$. The matched r.m.s. spot sizes and pulse lengths of the drive and trailing beams are $\sigma_{rd} = 10.37\,\mu$m and $\sigma_{rt} = 0.1\,\mu$m, and $\sigma_{zd} = 30\,\mu$m and $\sigma_{zt} = 10\,\mu$m respectively. The ratio $\frac{n_b}{n_0}$ of the trailing beam exceeds m_i/m_e for hydrogen so ion motion is expected to be an issue. Physically, ion motion occurs within the beam when the ion plasma frequency for the beam density, $\Omega_b = \sqrt{4\pi n_b e^2/m_i}$, times the beam duration exceeds unity, i.e., $\Omega_b \sigma_z/c >> 1$. This leads to the previous condition if $\sigma_z \approx c/\omega_p$. The two beams are separated by $115\,\mu$m, so that the trailing beam can flatten the longitudinal electric field E_z of the wake in order to maintain small energy spread [22], and the flattened $E_z \approx -1.0$.

We carried out a QuickPIC simulation using a box with $8192 \times 8192 \times 1024$ cells, and the resolution is $48.83\,nm \times 48.83\,nm \times 305.66\,nm$. In fig. 2a, 2D isosurface plots of the plasma and beam densities are shown for a slice along $y = 0$. The bubble radius is seen to be $\sim 3.5c/\omega_p \approx 54\mu$m, which is more than 500 times larger than σ_{rt}. This simulation also showed significant ion collapse as well as rapid emittance growth. However, there were only two cells across σ_{rt}. We therefore carried out simulations that only modeled a small volume (the dimensions are shown as a red box in fig. 2a) but with much higher resolution of $6.10\,nm \times 6.10\,nm \times 115.23\,nm$. The plasma was initialized as an ion column surrounded by a neutralizing and stationary electron sheath. We assume the drive beam does not contribute to the ion motion. The ion collapse and the focusing field on the trailing beam were nearly identical to that in the two-beam simulation with the same resolution [20].

In fig. 2b we show the ion (H^+) density behind the trailing beam (centered at $\xi = 0$) in the $y = 0$ slice. Following an initial spike, the peak ion density increases through the beam (along ξ), albeit with an oscillation to a maximum value around 200 times larger than n_0. The corresponding F_f is significantly perturbed around the axis as seen in fig. 2c where $\vec{F}_f \cdot \hat{x}$ in the y=0 plane is plotted for

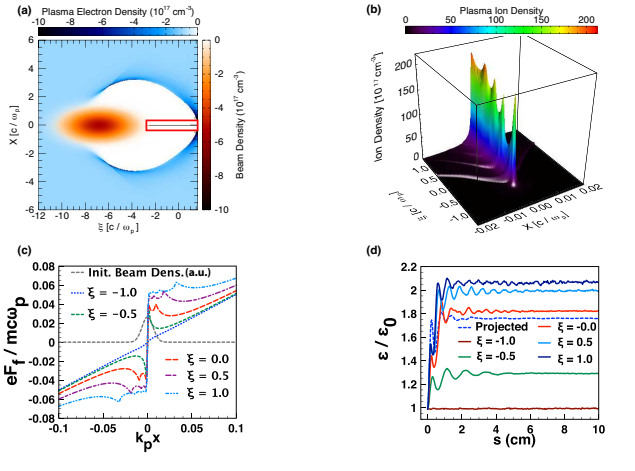

FIG. 2. PWFA with Ion motion:(a) Nonlinear wake in H plasma and the drive and trailing beam densities ($\xi = 0$ is the center of the trailing beam); (b) Plasma ion density in $x-\xi$ plane ($\xi = 0$ is the center of the trailing beam); (c) F_f transverse lineouts at different ξ and the initial beam density profile; (d) Trailing beam's projected and slice emittances evolution. The plasma skin depth is $k_p^{-1} = 16.83\,\mu$m in these plots.

several values of ξ. The slope of $\vec{F}_f \cdot \hat{x}$ is nearly the same in each slice, but the maximum value and width grows through the beam. The initial transverse density profile of the beam is shown as a reference. From fig. 2c, we can also estimate the perturbation of E_z using Panofsky-Wenzel theorem $\Delta E_z = \int dr \partial F_f/\partial\xi \approx \Delta r \Delta F_f / 2\Delta\xi$, which is on the order of 0.002 for $\Delta r = 0.1$, $\Delta F_f = 0.02$, and $\Delta\xi = 0.5$. The ΔE_z is negligible compared to -1.0 that felt by the trailing beam. This is consistent with the lower resolution simulations where the bubble excitation is also modeled. The basic reason for such a small perturbation on E_z is that for each slice the total charge contained in the ion density peak is very small and it changes slowly along ξ.

In fig. 2d, we plot the emittance growth for slices at the same values of ξ as well as the projected emittance. The emittance is seen to rapidly grow and then saturate for each slice. The projected emittance (and the slice in the middle of the beam) grows by less than a factor of 1.8 and slices in the rear of the beam only grow by a factor of 2.1. This emittance growth is much less than the anticipated growth [16, 17] and that seen in fig. 1b for A=200 and $\sigma = \sigma_{x0}$.

The fundamental reason for the significantly smaller than expected emittance growth is that the ion compression is much narrower than the initial beam spot size. This can be seen in fig. 3a, where a lineout of the ion density vs. x (for y=0) is shown in the middle of the beam, i.e., $\xi = 0$ is shown from the above simulation. For comparison, the initial trailing beam profile (dashed gray) as well as the prescribed form for the ion density (dashed red) for A=135.9 and $\sigma = 0.1\sigma_{x0}$ are also shown.

The narrower ion compression leads to a smaller value of p_{x0} and to an anharmonic motion such that the time average over a particles orbit is less than $p_{x0}/\sqrt{2}$. We note that the ion collapse develops a pedestal outside the core as one moves through the bunch although the width of the core remains unchanged. This effectively increases σ for the later slices.

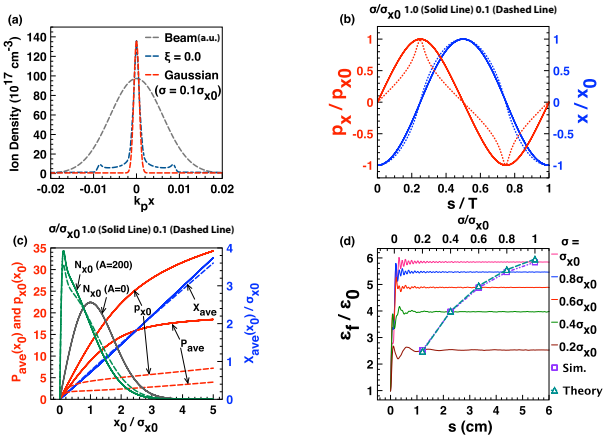

FIG. 3. (a) Plasma ion density lineout at $\xi = 0$ (blue dashed line) compared with the initial trailing beam distribution (grey dashed line) and a Gaussian fit for the core of the ion density (red dashed line); (b) p_x and x versus s in different focusing field (solid line for $\sigma/\sigma_{x0} = 1.0$ and dotted line for $\sigma/\sigma_{x0} = 0.1$) for the particle initially located at $x = \sigma_{x0}$;(c) $X_{\rm ave}(x_0)$, $P_{\rm ave}(x_0)$, $p_{x0}(x_0)$ and N_{x0} (in an arbitrary unit) in the focusing field with A =200 and different σ; (d) Slice beam emittance evolution in the focusing field with A =200 and different σ and final emittance growth from the simulation and theory.

To quantify the emittance growth, we first note that just as the emittance quickly reaches a steady state (as seen in fig. 2d) so too does the beam phase space and the ion density. In the steady state (where the spot size does not change), $<xp_x>_f = 0$, so the final emittance of the beam is $\epsilon_{Nxf} = \sqrt{<x^2>_f <p_x^2>_f}$. In addition, in the steady state $<x^2>_f = \{<x^2>\}_{t;\Delta t} = <\{x^2\}_{t;\Delta t}>$, where $\{\}_{t;\Delta t}$ represents the time average of a quantity at time t during a duration Δt. We can choose $\Delta t = T$ that is much larger than every particle's oscillation period τ. Therefore, $\{x^2\}_{t;T} = \{x^2\}_{t;\tau} \equiv X_{\rm ave}^2 = \frac{\int_0^{x_0} \frac{dx}{v_x} x^2}{\int_0^{x_0} \frac{dx}{v_x}} = \frac{\int_0^{x_0} dx\, x^2/\sqrt{(\psi(x,\xi)-\psi(x_0,\xi))}}{\int_0^{x_0} dx/\sqrt{(\psi(x,\xi)-\psi(x_0,\xi))}}$, where x_0 is the maximum value of x, $v_x = p_x/\gamma = \sqrt{2(\psi(x,\xi)-\psi(x_0,\xi))/\gamma}$, and ψ is the wake potential ($F_f(x) = -\partial\psi/\partial x$). For highly relativistic beams there is no phase slippage, so each slice evolves independently with a different phase space distribution. We henceforth assume that γ does not change so it can be brought out of the integrals. In reality, γ changes adiabatically, and including this in the numerical work does not alter the results. Following analogous reasoning leads to

$\{p_x^2\}_{t;T} = P_{\rm ave}^2 = \gamma \frac{\int_0^{x_0} dx \sqrt{(\psi(x,\xi)-\psi(x_0,\xi))}}{\int_0^{x_0} dx/\sqrt{(\psi(x,\xi)-\psi(x_0,\xi))}}$.

In fig. 3b, we plot p_x and x vs. $s = z \approx ct$ for an electron starting at rest at $x_0 = \sigma_{x0}$ in a focusing force with $A = 200$ and $\sigma = 0.1\sigma_{x0}$ or $\sigma = \sigma_{x0}$. The s axis is normalized to the period of the oscillation for each case, while the p_x and x are normalized to their maximum values p_{x0} and x_0. It is clearly seen that the $x(s)$ motion is essentially harmonic for both cases while the $p_x(s)$ motion is very different for the $\sigma = 0.1\sigma_{x0}$ (narrow ion collapse) case, i.e., it is anharmonic. Because the $x(s)$ motion is harmonic, $X_{\rm ave}/x_0 \approx 1/\sqrt{2}$ for both cases while by inspection of fig. 3b, $P_{\rm ave}/p_{x0} << 1/\sqrt{2}$ when $\sigma << \sigma_{x0}$. To quantify this, in fig. 3c we plot how $P_{\rm ave}$, p_{x0}, and $X_{\rm ave}$ depend on x_0 and σ for $A = 200$. This clearly shows that $P_{\rm ave}$ is much smaller than p_{x0} and that p_{x0} is much smaller when the ion collapse is narrower.

We now use $P_{\rm ave}$, $X_{\rm ave}$ and the initial beam distribution function, $f_0(x,p)$ to calculate $<x^2>_f$ and $<p^2>_f$. As mentioned before, $<x^2>_f = <X_{\rm ave}^2>$. To calculate $<X_{\rm ave}^2>$, we sort all the electrons by their orbits in phase space. All electrons with a maximum x value between x_0 and $x_0 + dx_0$, where $dx_0 << x_0$, will have the same $X_{\rm ave}^2(x_0)$. Therefore, $<x^2>_f = <X_{\rm ave}^2> = \frac{1}{N}\int_0^\infty dx_0 N_{x_0} X_{\rm ave}^2(x_0)$, where N is the total particle number and $N_{x_0}dx_0$ is the number of particles with orbits that have a maximum x between x_0 and $x_0 + dx_0$. N_{x_0} will not change in time, and according to its definition it can be calculated using $f_0(x,p)$. It follows that $N_{x0} = 4\int_0^{x_0} dx f_0(x,p_x)\frac{\partial p_x}{\partial x_0}$, where $\partial p_x/\partial x_0 = \sqrt{\gamma}F_f(x_0)/\sqrt{2(\psi(x)-\psi(x_0))}$. We can use f_0 since the ion collapse is in a quasi steady state even during the duration of the initial emittance growth. Following the same reasoning, we have $<p_x^2>_f = \frac{1}{N}\int_0^\infty dx_0 N_{x_0} P_{\rm ave}^2(x_0)$. In fig. 3c we also plot N_{x_0} for a case where there is no ion collapse ($A = 0$) and for $A = 200$ with different σ. This plot shows that when there is ion collapse the ensemble average is weighted towards particles with smaller x_0.

The final emittance (assuming 1D like motion) can be predicted for each slice using only ψ and f_0. In fig. 3d we show the predicted final emittance growth (compared with simulated results) for slices with initially Gaussian beams with matched spot sizes for the parameters described earlier. The curves correspond to different widths for the ion collapse with $A = 200$. The curves show significantly smaller emittance growth than what would be naively predicted from a $\sqrt{A}$ scaling.

In LC designs, asymmetric emittances are used to minimize the beamstrahlung [23] that occurs during disruption [24] at the final focus. In such a case, the ion collapse also becomes asymmetric and developing a model for the emittance growth is much more complicated. Therefore, we rely on highly resolved QuickPIC simulations. In fig. 4, we plot the emittance growth for a case where the initial emittances in the two transverse planes are $\epsilon_{Nx} = 2.0\,\mu$m, $\epsilon_{Ny} = 0.005\,\mu$m ($\sqrt{\epsilon_{Nx}\epsilon_{Ny}} = 0.1\,\mu$m is the same as the before). We still match the initial beam spot sizes to the $r/2$ focusing field, so that $\sigma_{rtx} = 463.9$ nm and $\sigma_{rty} = 23.2$ nm. The solid red and blue lines show the evolution of the trailing beam's projected emittances for a H^+ plasma.

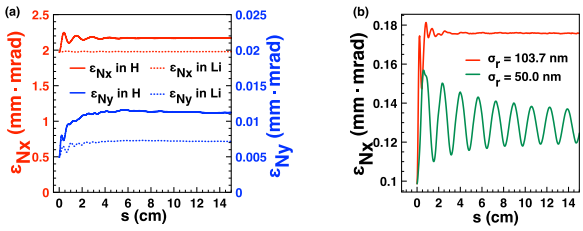

FIG. 4. Emittance Growth of (a) asymmetric beam in Hydrogen and Lithium; (b) symmetric beam with initially unmatched beam spot size in Hydrogen (compared with initially matched case).

It can be seen that the projected emittance growth in the plane with the larger emittance, ϵ_{Nx}, only grows by 10%. In the other plane, ϵ_{Ny} grows by 120%. Therefore the growth of $\sqrt{\epsilon_{Nx}\epsilon_{Ny}}$ is only 55.6% which is even smaller than the symmetric case. This appears to be mostly due to the fact that the peak ion density is smaller. To further mitigate the emittance growth, one could use a heavier ion, such as Li^+. In fig. 4a we show the emittance evolution of the same beam in a lithium plasma as the red and blue dotted lines. The emittance growth in the two planes is now less than 1% and 40% respectively, which are both reduced compared to the H^+ plasma. The growth of $\sqrt{\epsilon_{Nx}\epsilon_{Ny}}$ for Li^+ is only 18.9%. An issue for a Li plasma that requires further investigation is that the tightly focused trailing beam may further ionize the Li^+ ion if the transverse electric field exceeds $\sim$ 400 GV/m, which would cause additional modifications to the focusing force.

Another way to mitigate emittance growth is to use an initial beam spot size less than the matched spot size (over focused) for fixed ions but closer to the steady state value when there is ion collapse. Fig. 4b shows the projected emittance growth for a symmetric beam with an initially unmatched spot size. The beam has the same initial emittance as used to generate fig. 2, but it had a smaller spot size $\sigma_{rt} = 50.0$ nm. The projected emittance growth is substantially less but it now appears to oscillate. The amplitude of the oscillations is decreasing over time indicating that a steady state is being approached with a final emittance growth of only $\sim$ 25%. Finally we note that in a PWFA-LC a series of stages will be used. These results indicate that the emittance growth might only occur in the first stage and that once the steady state is formed the emittance will not grow in later stages if the beam can be properly transported into and out of the additional stages.

This work was supported by the US Department of Energy under grants DE-SC0010064, DE-SC0008491, DE-SC0008316, DE-SC0014260, and NSF grants ACI-1339893, PHY-1500630. The simulations were carried out on the Blue Waters under the NSF grant ACI-1440071 and the UCLA Hoffman 2 and Dawson 2 Clusters.

* anweiming@ucla.edu

[1] C. G. R. Geddes *et al.*, Nature **431**, 538 (2004).
[2] J. Faure *et al.*, Nature **431**, 541 (2004).
[3] S. P. D. Mangles *et al.*, Nature **431**, 535 (2004).
[4] W. P. Leemans *et al.*, Nature Phys. **696**, 2 (2006).
[5] I. Blumenfeld *et al.*, Nature **445**, 741 (2007).
[6] M. Litos *et al.*, Nature **92**, 515 (2014).
[7] W. P. Leemans *et al.*, Phys. Rev. Lett. **113**, 245002 (2014).
[8] S. Corde *et al.*, Nature **524**, 442 (2015).
[9] A. Seryi *et al.*, in *Proceedings of the 2009 PAC Conference, Vancouver, BC, Canada* (AIP, NY, 2009).
[10] E. Adli *et al.*, arXiv:1308.1145 (2013).
[11] W. Leemans and E. Esarey, Physics Today **62**, 44 (2009).
[12] J. B. Rosenzweig *et al.*, Phys. Rev. A **44**, R6189 (1991).
[13] W. Lu *et al.*, Phys. Rev. Lett. **96**, 165002 (2006).
[14] W. Lu *et al.*, Phys. Plasmas **13**, 056709 (2006).
[15] C. Joshi *et al.*, Phys. Plasmas **9**, 1845 (2002).
[16] J. B. Rosenzweig *et al.*, Phys. Rev. Lett. **95**, 195002 (2005).
[17] R. Gholizadeh *et al.*, Phys. Rev. Lett. **104**, 155001 (2010).
[18] C. Huang *et al.*, J. Comp. Phys. **217**, 658 (2006).
[19] W. An *et al.*, J. Comp. Phys. **250**, 165 (2013).
[20] See Supplemental Material at [URL] for QuickPIC and its simulation.
[21] C. Huang *et al.*, in *Proceedings of the 2009 PAC Conference, Vancouver, BC, Canada* (AIP, NY, 2009).
[22] M. Tzoufras *et al.*, Phys. Rev. Lett. **101**, 145002 (2008).
[23] M. Bell and J. S. Bell, Part. Accl. **24**, 1 (1988).
[24] P. Chen and K. Yokoya, Phys. Rev. D **38**, 987 (1988).